Correlated fluorescence microscopy and multi-ion beam secondary ion mass spectrometry imaging reveals phosphatidylethanolamine increases in the membrane of cancer cells over-expressing the molecular chaperone subunit CCTd

APPLIED PHYSICS

Generating spatially entangled itinerant photons with waveguide quantum electrodynamics

B. Kannan[1,2]*, D. L. Campbell[1], F. Vasconcelos[1,2], R. Winik[1], D. K. Kim[3], M. Kjaergaard[1], P. Krantz[1†], A. Melville[3], B. M. Niedzielski[3], J. L. Yoder[3], T. P. Orlando[1,2], S. Gustavsson[1], W. D. Oliver[1,2,3,4]

Realizing a fully connected network of quantum processors requires the ability to distribute quantum entanglement. For distant processing nodes, this can be achieved by generating, routing, and capturing spatially entangled itinerant photons. In this work, we demonstrate the deterministic generation of such photons using superconducting transmon qubits that are directly coupled to a waveguide. In particular, we generate two-photon N00N states and show that the state and spatial entanglement of the emitted photons are tunable via the qubit frequencies. Using quadrature amplitude detection, we reconstruct the moments and correlations of the photonic modes and demonstrate state preparation fidelities of 84%. Our results provide a path toward realizing quantum communication and teleportation protocols using itinerant photons generated by quantum interference within a waveguide quantum electrodynamics architecture.

INTRODUCTION

Modular architectures of quantum computing hardware have recently been proposed as an approach to realize robust large-scale quantum information processing (*1*–*4*). However, such architectures rely on a means to coherently transfer quantum information between individual, and generally nonlocal, processing nodes. Spatially entangled itinerant photons can be used to achieve this by efficiently distributing entanglement throughout a quantum network. Conventional approaches for generating such photons in optical systems typically use spontaneous parametric down conversion in conjunction with arrays of beamsplitters (*5*) and photodetectors for postselection (*6*, *7*). However, the stochastic nature of these approaches limits their utility in quantum information processing applications.

Recent progress with superconducting circuits has established a path toward realizing a universal quantum node that is capable of storing, communicating, and processing quantum information (*8*–*12*). These works often invoke a cavity quantum electrodynamics (cQED) architecture, where cavities protect qubits from decoherence within a node, enabling the high-fidelity control required to generate arbitrary quantum states. To link distant nodes, this quantum information must propagate along a bus composed of a continuum (or quasi-continuum) of modes. To this end, we strongly couple qubits to a waveguide such that the excitations stored in the qubits are rapidly released as itinerant photons. Such a system is described by waveguide quantum electrodynamics (wQED). Entering the strong coupling regime in wQED enables qubits to serve as high-quality quantum emitters (*13*). More generally, superconducting circuits have been used to produce a wide variety of nonclassical itinerant photons from classical drives (*14*–*18*), such as those with correlations and entanglement in frequency (*18*).

Here, we demonstrate that the indistinguishability and quantum interference between photons directly emitted from multiple sources into a waveguide can deterministically generate spatially entangled itinerant photons. In particular, we generate two-photon N00N states $|\psi_{ph}\rangle = (|20\rangle - |02\rangle)/\sqrt{2}$, where the state $|n_L n_R\rangle$ denotes the number of photons in the left and right propagating modes of the waveguide, respectively. More generally, we show that our device can generate itinerant photons with states of the form $|\psi_{ph}\rangle = a|20\rangle + b|02\rangle + c|11\rangle$, where a, b, and c are complex coefficients that are set by the effective qubit spatial separation Δx.

RESULTS

Device description and photon generation protocol

The test device consists of three flux-tunable transmon qubits (*19*) that are capacitively coupled to a common 50-ohm transmission line (an electromagnetic coplanar waveguide), as shown in Fig. 1A. The configurations we consider involve two qubits, used as photonic emitters, that are spatially separated by $\Delta x = 3\lambda/4$ and $\Delta x = \lambda/2$. The effective spacing is controlled by the qubit frequencies ω (*20*) via the corresponding wavelengths $\lambda = 2\pi v/\omega$, where v is the speed of light in the waveguide. Setting the transition frequencies of qubits Q_1 and Q_3 to $\omega/2\pi = 4.85$ GHz corresponds to a spacing of $\Delta x = 3\lambda/4$ between emitters. The frequency of the central qubit Q_2 is detuned hundreds of megahertz such that it can be ignored. In this configuration, the qubits are coupled to the coplanar waveguide with a coupling strength of $\gamma/2\pi = 0.53$ MHz. Alternatively, to realize a spacing of $\Delta x = \lambda/2$ between emitters, the frequencies of Q_1 and Q_2 are set to $\omega/2\pi = 6.45$ GHz, where the qubit-waveguide coupling strength is $\gamma/2\pi = 0.95$ MHz, while sufficiently detuning Q_3 so that it may be ignored.

The Hamiltonian of the qubit-waveguide system is (*21*)

$$\hat{H} = \int_0^\infty d\omega \hbar\omega \left[\hat{a}_L^\dagger(\omega)\hat{a}_L(\omega) + \hat{a}_R^\dagger(\omega)\hat{a}_R(\omega)\right] + \sum_j \frac{\hbar\omega_j}{2}\hat{\sigma}_z^{(j)} - i\sum_j \int_0^\infty d\omega \hbar g_j(\omega)\left[\hat{a}_L^\dagger(\omega)e^{-i\omega x_j/v} + \hat{a}_R^\dagger(\omega)e^{i\omega x_j/v} + \text{h.c.}\right]\hat{\sigma}_x^{(j)} \quad (1)$$

[1]Research Laboratory of Electronics, Massachusetts Institute of Technology, Cambridge, MA 02139, USA. [2]Department of Electrical Engineering and Computer Science, Massachusetts Institute of Technology, Cambridge, MA 02139, USA. [3]MIT Lincoln Laboratory, 244 Wood Street, Lexington, MA 02420, USA. [4]Department of Physics, Massachusetts Institute of Technology, Cambridge, MA 02139, USA.
*Corresponding author. Email: bkannan@mit.edu
†Present address: Wallenberg Centre for Quantum Technology, Department of Microtechnology and Nanoscience, Chalmers University of Technology, Gothenburg, Sweden.

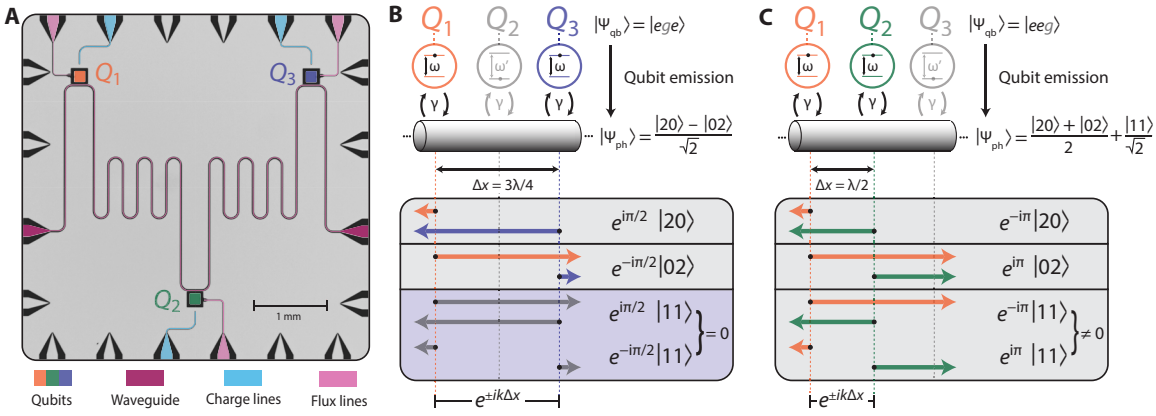

Fig. 1. Generating spatially correlated itinerant photons in wQED. (**A**) False-colored micrograph of the device. The device consists of three independently flux-tunable transmon qubits that are capacitively coupled to a common waveguide. (**B**) Schematic diagram of three qubits that are coupled to a common waveguide with equal strength γ. Qubits Q_1 and Q_3 are initially excited and placed on resonance at $\omega/2\pi = 4.85$ GHz such that their spatial separation along the waveguide is $\Delta x = 3\lambda/4$. Qubit Q_2 is detuned far away $|\omega' - \omega| \gg \gamma$ such that it can be ignored and is left in the ground state. The four possible coherent pathways for the photons emitted by the qubits into the left and right traveling modes of the waveguide are shown below. The state of the emitted photons is a two-photon N00N state due to destructive interference between the single-photon pathways $|11\rangle$. (**C**) Same setup as (B) except Q_1 and Q_2 are now placed on resonance $\omega/2\pi = 6.45$ GHz such that $\Delta x = \lambda/2$ and Q_3 is now detuned far away. The $|11\rangle$ states constructively interfere for this choice of Δx.

where $\hat{a}^{\dagger}_{L(R)}(\omega)$ and $\hat{a}_{L(R)}(\omega)$ are the creation and annihilation operators for left (right) propagating photons in the waveguide with frequency ω, x_j is the position of the j^{th} qubit, and $\hat{\sigma}^{(j)}_x$ and $\hat{\sigma}^{(j)}_z$ are the qubit X and Z Pauli operators. The coupling strength $g_j(\omega)$ determines the physical qubit-waveguide coupling rate $\gamma(\omega_j) = 4\pi g_j(\omega_j)^2 D(\omega_j)$, where $D(\omega)$ is the density of photonic modes in the waveguide. The qubits couple to the transmission line with equal strength when placed on resonance with each other.

When the propagation time for photons between the qubits is small relative to the time scale γ^{-1} of the qubit emission, the system can be simulated for arbitrary initial conditions and spacings by integrating a master equation derived from the Hamiltonian in Eq. 1 and applying input-output theory (*21*). The input-output relations that provide the dynamics of the photons emitted into the left- and right-propagating modes are

$$\hat{a}_L(t) = \hat{a}^{\text{in}}_L(t) + \sqrt{\frac{\gamma}{2}}\left(\hat{\sigma}^{(1)}_- + \hat{\sigma}^{(2)}_- e^{\frac{-i\omega\Delta x}{v}}\right)$$
$$\hat{a}_R(t) = \hat{a}^{\text{in}}_R(t) + \sqrt{\frac{\gamma}{2}}\left(\hat{\sigma}^{(1)}_- + \hat{\sigma}^{(2)}_- e^{\frac{i\omega\Delta x}{v}}\right) \quad (2)$$

where $\hat{a}^{\text{in}}_{L/R}(t)$ are the incoming field operators at time t whose corresponding fields are taken to be in the vacuum state.

The two resonant qubits in each spacing configuration are initialized to their excited states, while the detuned qubit is left in the ground state. Under these conditions, the final (unnormalized) state of the photons emitted by the excited qubits is given by

$$|\psi_{\text{ph}}\rangle \otimes |gg\rangle = \prod_j^2 (\hat{a}^{\dagger}_L e^{-i\omega x_j/v} + \hat{a}^{\dagger}_R e^{i\omega x_j/v})|00\rangle \otimes \hat{\sigma}^{(j)}_- |ee\rangle \quad (3)$$

where the photonic modes $\hat{a}^{\dagger}_{L(R)}$ have been integrated over the time coordinate such that they are time independent, and the index j is multiplied over the two active qubits that are prepared in the state $|ee\rangle$ (Q_1, Q_3 for $\Delta x = 3\lambda/4$ and Q_1, Q_2 for $\Delta x = \lambda/2$). From Eq. 3, we may verify that $|\psi_{\text{ph}}\rangle$ is a two-photon N00N state when the spatial separation between qubits is $\Delta x = \lambda/4, 3\lambda/4, \ldots, (2n+1)\lambda/4$, where n is an integer. This can be understood by considering the interference between the four possible coherent emission pathways for two excitations to leave the system (shown in Fig. 1B). The emission pathways containing a single photon in both the left and right propagating modes destructively interfere, resulting in the entangled state $|\psi_{\text{ph}}\rangle = (|20\rangle - |02\rangle)/\sqrt{2}$. Note that waveguide-mediated exchange interactions can be ignored because both qubits are fully excited. In contrast, for spacings $\Delta x = 0, \lambda/2, \ldots, n\lambda/2$, depicted in Fig. 1C, the destructive interference no longer occurs, resulting in a standard (equal) partitioning of the photons into the left and right propagating modes. For this latter configuration, the decay of the qubits from $|ee\rangle$ to $|gg\rangle$ is determined by super-radiant emission (*20*).

Measurement techniques and protocols

Figure 2A shows the control and measurement schematic. First, we measure the scattering of coherent microwave fields to extract qubit parameters and calibrate the absolute power of photons at the qubit (see the Supplementary Materials). Next, we independently prepare the qubits by detuning them from each other and then applying resonant microwave pulses to the transmission line. The qubits can be individually prepared anywhere on the Bloch sphere $\alpha|g\rangle + \beta|e\rangle$, where α and β are complex coefficients determined by the amplitude and phase of the pulse. We then verify the state of the photons that are emitted by the qubits using quadrature amplitude detection of the left and right outputs of the transmission line. These photons are amplified and downconverted to an intermediate frequency f_d using in-phase and quadrature (IQ) mixing. For example, we can prepare a single detuned qubit in the state $(|g\rangle + |e\rangle)/\sqrt{2}$, which we use for calibration purposes (see below), and capture the time dynamics of the emission (Fig. 2B) by averaging the voltage amplitudes $V^{I/Q}_{L/R}(t)$ at the output of the IQ mixers over many records. The qubit can also be fully excited to $|e\rangle$, as will be required for the N00N-state generation protocol. In this case, the emitted photon has no coherence relative to the vacuum state $|00\rangle$, and thus, the voltage averages to zero as shown in Fig. 2C.

To uniquely identify the state and correlations of the photons emitted from two qubits, it is necessary to measure higher-order

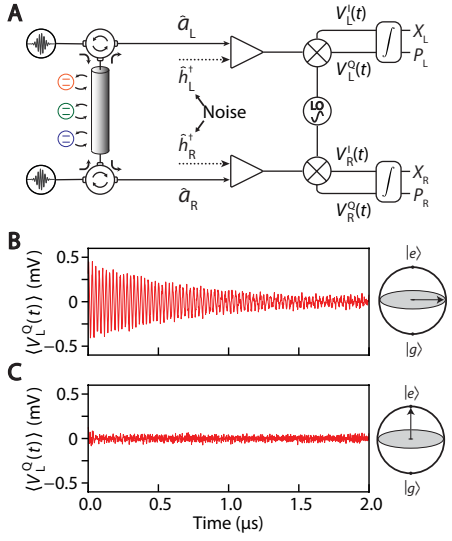

Fig. 2. Measurement setup and procedure. (**A**) Schematic setup of the dual-sided control and measurement chain. The signal from the photons emitted by the qubits is amplified and downconverted to an intermediary frequency f_d before digitization. The digitized signal is then further demodulated and integrated using custom field-programmable gate array (FPGA) code to obtain a pair of complex numbers $S_L = X_L + iP_L$ and $S_R = X_R + iP_R$. Single-shot measurements of these values are then binned into a histogram to construct a 4D probability distribution. The mode of interest, $\hat{a}_{L(R)}$, and noise mode, $\hat{h}^\dagger_{L(R)}$, of the left (right) measurement chain are indicated directly before amplification. (**B**) Representative time trace of the digitized and averaged voltage from the emission of a single qubit initialized to $(|g\rangle + |e\rangle)/\sqrt{2}$. The exponential temporal envelope of the emission is superimposed with oscillations at the downconverted frequency $f_d = 40$ MHz. (**C**) Voltage from the emission of a qubit initialized to $|e\rangle$. The photon is emitted with a random phase such that the voltage averages to zero.

moments of the fields. To do this, time-independent values for the field quadratures of both the left $S_L = X_L + iP_L$ and right $S_R = X_R + iP_R$ emission signals are obtained through digital demodulation and integration of individual records of $V^{I/Q}_{L/R}(t)$. Using repeated measurements of these values, we construct a four-dimensional (4D) probability distribution $Q(S_L, S_L^*, S_R, S_R^*)$ that are used to obtain the moments of S_L and S_R

$$\langle \hat{S}_L^{\dagger w} \hat{S}_L^x \hat{S}_R^{\dagger y} \hat{S}_R^z \rangle = \int d^2 S_L \, d^2 S_R \, S_L^{*w} S_L^x S_R^{*y} S_R^z \, Q(S_L, S_L^*, S_R, S_R^*) \quad (4)$$

We account for the noise added by the amplifiers in the measurement chain by using the input-output relations for a phase-insensitive amplifier $\hat{S}_{L(R)} = \sqrt{G_{L(R)}}\,\hat{a}_{L(R)} + \sqrt{G_{L(R)} - 1}\,\hat{h}^\dagger_{L(R)}$ (*22*–*24*), where $\hat{a}_{L(R)}$ is the left (right) output mode of the device, $\hat{h}^\dagger_{L(R)}$ is the noise mode added by the left (right) amplification chain, and $G_{L(R)}$ is the gain of the left (right) amplification chain. The moments of the noise channels $\langle \hat{h}_L^w \hat{h}_L^{\dagger x} \hat{h}_R^y \hat{h}_R^{\dagger z} \rangle$ are found by measuring the moments of S_L and S_R while leaving the qubits in the ground state. We account for residual thermal photons with an effective temperature ≈46 mK in $\hat{a}_{L,R}$ when computing the moments of $\hat{h}^\dagger_{L(R)}$. The moments of the fields before amplification $\langle \hat{a}_L^{\dagger w} \hat{a}_L^x \hat{a}_R^{\dagger y} \hat{a}_R^z \rangle$ are then determined by inverting the amplifier input-output relations (see Materials and Methods).

Before generating the photonic states of interest, we first obtain the properties of the measurement chains. We are able to calibrate the net amplification gain by preparing a single qubit in an equal superposition of its ground and excited states (*22*), as done in Fig. 2B. For this case, provided the qubits are prepared with a sufficiently high fidelity, the state of the emitted photon will approximately be $|00\rangle/\sqrt{2} + (|10\rangle + |01\rangle)/2$ since the photon is released symmetrically into both outputs of the waveguide. By taking advantage of the difference in scaling between first- and second-order moments with respect to $G_{L(R)}$, the gain can be calibrated by finding the value for which $\langle \hat{a}_{L(R)} \rangle = \sqrt{2}\langle \hat{a}^\dagger_{L(R)} \hat{a}_{L(R)} \rangle$ is obtained from the inverted input-output relations of the amplifiers. Next, because the statistics of the noise modes are well described by a thermal state $\hat{\rho}_h = \sum_i n^i_{noise}/(1 + n_{noise})^{i+1} |i\rangle\langle i|$, where n_{noise} is the average number of photons added by the noise, we can find the detection efficiency of our measurement chains $\eta = (1 + n_{noise})^{-1}$ by performing a maximum likelihood estimation on the measured moments of $\hat{h}_{L,R}$. We extract the n_{noise} that best describes the measurements and find the detection efficiencies to be $\eta_{L(R)} \approx 10.4\,\%$ (12.1 %). Finally, we alternate between initializing the qubits in the fully excited ($|ee\rangle$) and ground ($|gg\rangle$) states while measuring $\hat{S}_{L(R)}$ with a repetition period of 10 μs to obtain the statistics of the emitted photons and the noise.

Photon state verification via state tomography

We first initialize the qubits to $|\psi_{qb}\rangle = |ege\rangle$ with Q_1 and Q_3 separated by a distance of $\Delta x = 3\lambda/4$ along the waveguide. In doing so, we generate the two-photon N00N state $|\psi_{ph}\rangle = (|20\rangle - |02\rangle)/\sqrt{2}$ because of the complete destructive quantum interference of the $|11\rangle$ state, given by the phase factors shown in Fig. 1B. This is reminiscent of the final-state stimulation due to bosonic quantum statistics that is observed with identical photons in a Hong-Ou-Mandel experiment (*25*, *26*). We are able to validate the state of the emitted photons through the moments and correlations between the left and right output modes shown in Fig. 3A. We observe $\langle \hat{a}_L^\dagger \hat{a}_L \rangle \approx \langle \hat{a}_R^\dagger \hat{a}_R \rangle \approx 1$, since there is one photon per mode on average. We also observe that the two-photon coincidences are $\langle \hat{a}_L^{\dagger 2} \hat{a}_L{}^2 \rangle \approx \langle \hat{a}_R^{\dagger 2} \hat{a}_R{}^2 \rangle \approx 1$, whereas the cross-coincidence is $\langle \hat{a}_L^\dagger \hat{a}_L \hat{a}_R^\dagger \hat{a}_R \rangle \approx 0$. These moments are consistent with two photons simultaneously arriving at the same detector rather than a single photon at each. Coherence between the $|20\rangle$ and $|02\rangle$ states is demonstrated via the two-photon cross-correlation $\langle \hat{a}_L{}^2 \hat{a}_R^{\dagger 2} \rangle \approx -1$.

We contrast the case of $\Delta x = 3\lambda/4$ with $\Delta x = \lambda/2$ to demonstrate the tunability of $|\psi_{ph}\rangle$. Here, we use Q_1 and Q_2 and initialize the qubits to $|\psi_{qb}\rangle = |eeg\rangle$. Constructive quantum interference of $|11\rangle$ leads to the output state $|\psi_{ph}\rangle = (|20\rangle + |02\rangle)/2 + |11\rangle/\sqrt{2}$ (Fig. 1C). The statistics of $|\psi_{ph}\rangle$ are now consistent with the standard partitioning of two classical particles, with each being independently and equally likely to appear in one of the two modes. The moments for this case are shown in Fig. 3B and once again verify the predicted outcome. We obtain $\langle \hat{a}_L^\dagger \hat{a}_L \rangle \approx \langle \hat{a}_R^\dagger \hat{a}_R \rangle \approx 1$ as the average number of photons per mode remains unity. However, the two photons will now occupy the same mode only half of the time. As a result, two-photon coincidences $\langle \hat{a}_L^{\dagger 2} \hat{a}_L{}^2 \rangle \approx \langle \hat{a}_R^{\dagger 2} \hat{a}_R{}^2 \rangle \approx 1/2$ only occur 50% of the time, compared with 100% of the time for the two-photon N00N state. In addition, we now observe a nonzero cross-coincidence $\langle \hat{a}_L^\dagger \hat{a}_L \hat{a}_R^\dagger \hat{a}_R \rangle \approx 0.5$, indicating that the photons arrive at opposite detectors the other 50% of the time. Finally, the measurements of $\langle \hat{a}_L \hat{a}_R^\dagger \rangle \approx 1, \langle \hat{a}_L{}^2 \hat{a}_R^{\dagger 2} \rangle \approx 0.5$, and $\langle \hat{a}_L \hat{a}_R^{\dagger 2} \hat{a}_R^\dagger \rangle \approx \langle \hat{a}_L^\dagger \hat{a}_L{}^2 \hat{a}_R^\dagger \rangle \approx 0.5$ demonstrate the appropriate coherences between the $|02\rangle$, $|20\rangle$, and $|11\rangle$ states.

To further characterize the state of the emitted photons, we obtain the density matrix $\hat{\rho}$ in the Fock-state basis by applying

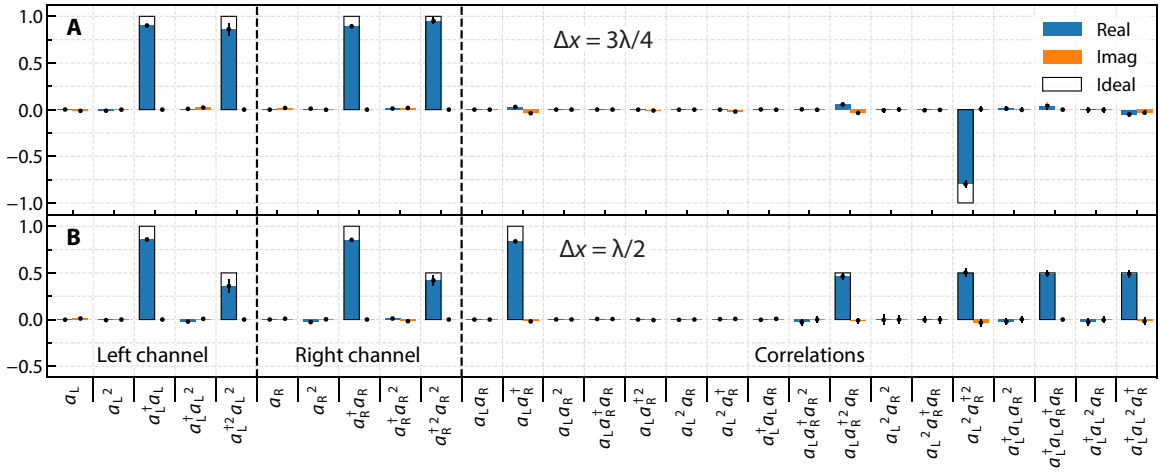

Fig. 3. Photon state tomography. (**A**) Real (blue) and imaginary (orange) parts of the measured normally ordered moments of the left and right propagating photonic fields $\langle \hat{a}_L^{\dagger w} \hat{a}_L^{x} \hat{a}_R^{\dagger y} \hat{a}_R^{z} \rangle$ up to fourth order ($w, x, y, z \in \{0,1,2\}$) for $\Delta x = 3\lambda/4$. The moments are separated according to their corresponding channel or correlations. The ideal values for the moments are given by the box frames around the measured values. (**B**) Measured and ideal moments for $\Delta x = \lambda/2$.

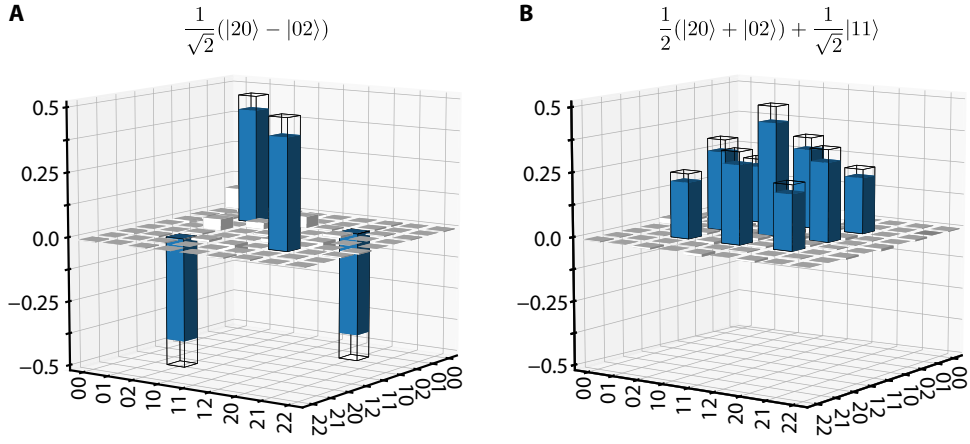

Fig. 4. Density matrix reconstruction of photonic states. Real part of the density matrix in the Fock basis of the left and right propagating modes compared with the expected state (wire frames) for (**A**) $(|20\rangle - |02\rangle)/\sqrt{2}$ at $\Delta x = 3\lambda/4$ and (**B**) $(|20\rangle + |02\rangle)/2 + |11\rangle/\sqrt{2}$ at $\Delta x = \lambda/2$. Density matrices are obtained via maximum likelihood estimation on measured photonic moments with fidelities of 84 and 87%, respectively. The matrix elements that are ideally nonzero are shaded in blue. The predominant source of infidelity is given by the finite population of 0.09 (A) and 0.11 (B) in the $|00\rangle\langle 00|$ state.

maximum likelihood estimation to the measured moments. The real part of $\hat{\rho}$ is shown in Fig. 4, with the magnitude of all values in the imaginary part (not shown) being less than 0.037. The N00N state generated with $\Delta x = 3\lambda/4$ is evident in Fig. 4A with a trace overlap fidelity of $\mathrm{Tr}(\hat{\rho}\hat{\sigma}) = 84\%$, where $\hat{\sigma}$ is the ideal density matrix. The density matrix for the emitted photons at $\Delta x = \lambda/2$ is shown in Fig. 4B with a state preparation fidelity of 87%. In both cases, we attribute the majority of the infidelity to waveguide-induced T_1 decay of the qubits during the state initialization, as evidenced by a finite population of 0.09 and 0.11 in the $|00\rangle$ state of $\hat{\rho}$. Recent work has shown that this infidelity can be substantially reduced with the use of quantum inference with "giant atoms" (*27*, *28*), where qubit-waveguide couplings can be tuned in situ such that the qubits are not subject to waveguide-induced decoherence during state preparation. Furthermore, giant atoms can also be used to engineer tailored qubit-waveguide coupling, waveguide-mediated qubit-qubit coupling, and correlated decay spectra (*28*) with the desired properties for a given interference condition.

DISCUSSION

Our results demonstrate that a wQED architecture supports the high-fidelity generation of spatially entangled microwave photons. Our approach is extensible to higher-order photonic states through the addition of qubits, such that more photons are emitted, and with the appropriate choices of Δx to obtain the desired quantum interference. These types of photonic states are also known to be useful for high-precision phase measurements in quantum metrology (*29*). Although current limitations in detector efficiency hinder the ability to measure higher-order moments, and thus verify the resulting higher-order photonic states, recent proposals for number-resolved microwave photon detectors (*30*, *31*) can address this issue. Finally, devices of the type studied in this work can be further generalized with the addition of direct qubit-qubit coupling, which can be used to dynamically select the direction in which photons are emitted or absorbed (*32*). We envision an architecture where quantum information and entanglement are routed and spread throughout a

quantum network via the quantum interference between the photons emitted by qubits that are coupled to a waveguide. Generating itinerant photons using the principles and techniques outlined in this work can then be applied toward realizing interconnected quantum networks for both quantum communication and distributed quantum computation.

MATERIALS AND METHODS

Moment inversion

We describe an efficient procedure for determining the moments of the field before amplification, $\langle \hat{a}_L^{\dagger n} \hat{a}_L^m \hat{a}_R^{\dagger k} \hat{a}_R^l \rangle$, where $n, m, k, l \in \{0, N\}$ are integers up to a desired moment order N. In our experiment, we consider moments of order up to $N = 2$. The standard input-output relationship for phase-insensitive amplifiers is given by

$$\hat{S}_{L(R)} = \sqrt{G_{L(R)}}\,\hat{a}_{L(R)} + \sqrt{G_{L(R)} - 1}\,\hat{h}_{L(R)}^{\dagger} \tag{5}$$

where $\hat{a}_{L(R)}$ is the left (right) output mode of the device, $\hat{h}_{L(R)}^{\dagger}$ is the noise mode added by the left (right) amplification chain, and $G_{L(R)}$ is the amplification of the left (right) amplification chain (*22*–*24*). When the gain of the amplifiers are large ($G_{L(R)} \gg 1$), as is the case in our setup, Eq. 4 can be simplified to

$$\hat{S}'_{L(R)} = \frac{\hat{S}_{L(R)}}{\sqrt{G_{L(R)}}} \approx \hat{a}_{L(R)} + \hat{h}_{L(R)}^{\dagger} \tag{6}$$

Furthermore, we assume that modes of interest $\hat{a}_{L(R)}$ and noise modes $\hat{h}_{L(R)}$ are uncorrelated. Under these conditions, the moments of $\hat{S}'_{L(R)}$, $\hat{a}_{L(R)}$, and $\hat{h}_{L(R)}^{\dagger}$ are related as

$$\begin{aligned}\langle \hat{S}_L'^{\dagger n} \hat{S}_L'^{m} \hat{S}_R'^{\dagger k} \hat{S}_R'^{l} \rangle = \sum_{w=0}^{n}\sum_{x=0}^{m}\sum_{y=0}^{k}\sum_{z=0}^{l} \binom{n}{w}\binom{m}{x}\binom{k}{y}\binom{l}{z} \\ \langle \hat{a}_L^{\dagger w} \hat{a}_L^{x} \hat{a}_R^{\dagger y} \hat{a}_R^{z} \rangle \langle \hat{h}_L^{n-w} \hat{h}_L^{\dagger m-x} \hat{h}_R^{k-y} \hat{h}_R^{\dagger l-z} \rangle\end{aligned} \tag{7}$$

As described in the measurement techniques and protocols section, we use heterodyne detection on the output of the measurement chain to form a 4D probability distribution, $Q(S_L, S_L^*, S_R, S_R^*)$, from which the moments of S'_L and S'_R can be obtained

$$\langle \hat{S}_L'^{\dagger n} \hat{S}_L'^{m} \hat{S}_R'^{\dagger k} \hat{S}_R'^{l} \rangle = \int d^2 S_L\, d^2 S_R\, S_L^{*n} S_L^{m} S_R^{*k} S_R^{l}\, Q(S_L, S_L^*, S_R, S_R^*)\, G_L^{-\frac{n+m}{2}} G_R^{\frac{k+l}{2}} \tag{8}$$

To obtain the moments of the noise added by the amplifiers $\langle \hat{h}_L^n \hat{h}_L^{\dagger m} \hat{h}_R^k \hat{h}_R^{\dagger l} \rangle$, the qubits are left in their ground states. If the temperature of $\hat{a}_{L/R}$ is small $k_B T \ll \hbar\omega$, then the state of these photonic modes can be approximated as vacuum. Under these conditions, we have

$$\langle \hat{a}_L^{\dagger w} \hat{a}_L^{x} \hat{a}_R^{\dagger y} \hat{a}_R^{z} \rangle = \begin{cases} 1 & \text{if } w, x, y, z = 0 \\ 0 & \text{otherwise} \end{cases}. \tag{9}$$

Equation 6 is then significantly reduced such that moments of the noise channels can be directly obtained from the measured moments of $\langle \hat{S}_L'^{\dagger n} \hat{S}_L'^{m} \hat{S}_R'^{\dagger k} \hat{S}_R'^{l} \rangle_0$ with $|\psi_{ph}\rangle = |00\rangle$

$$\langle \hat{h}_L^n \hat{h}_L^{\dagger m} \hat{h}_R^k \hat{h}_R^{\dagger l} \rangle = \langle \hat{S}_L'^{\dagger n} \hat{S}_L'^{m} \hat{S}_R'^{\dagger k} \hat{S}_R'^{l} \rangle_0 \tag{10}$$

After determining both $\langle \hat{S}_L'^{\dagger n} \hat{S}_L'^{m} \hat{S}_R'^{\dagger k} \hat{S}_R'^{l} \rangle$ and $\langle \hat{h}_L^n \hat{h}_L^{\dagger m} \hat{h}_R^k \hat{h}_R^{\dagger l} \rangle$, we can solve for $\langle \hat{a}_L^{\dagger w} \hat{a}_L^{x} \hat{a}_R^{\dagger y} \hat{a}_R^{z} \rangle$ by inverting a system of linear equations. We begin by defining vectors $\vec{S}$ and $\vec{a}$, where the elements are all possible combinations of $\langle \hat{S}_L'^{\dagger n} \hat{S}_L'^{m} \hat{S}_R'^{\dagger k} \hat{S}_R'^{l} \rangle$ and $\langle \hat{a}_L^{\dagger w} \hat{a}_L^{x} \hat{a}_R^{\dagger y} \hat{a}_R^{z} \rangle$, respectively. These vectors are length $(N+1)^4$ and takes the form

$$\vec{S} = \begin{bmatrix} 1 \\ \langle \hat{S}'_R \rangle \\ \langle \hat{S}_R'^{2} \rangle \\ \vdots \\ \langle \hat{S}_R'^{N} \rangle \\ \langle \hat{S}_R'^{\dagger} \rangle \\ \langle \hat{S}_R'^{\dagger} \hat{S}'_R \rangle \\ \vdots \\ \langle \hat{S}_R'^{\dagger N} \hat{S}_R'^{N} \rangle \\ \vdots \\ \langle \hat{S}_L'^{N} \hat{S}_R'^{\dagger N} \hat{S}_R'^{N} \rangle \\ \vdots \\ \langle \hat{S}_L'^{\dagger N} \hat{S}_L'^{N} \hat{S}_R'^{\dagger N} \hat{S}_R'^{N} \rangle \end{bmatrix}, \vec{a} = \begin{bmatrix} 1 \\ \langle \hat{a}_R \rangle \\ \langle \hat{a}_R^2 \rangle \\ \vdots \\ \langle \hat{a}_R^N \rangle \\ \langle \hat{a}_R^{\dagger} \rangle \\ \langle \hat{a}_R^{\dagger} \hat{a}_R \rangle \\ \vdots \\ \langle \hat{a}_R^{\dagger N} \hat{a}_R^N \rangle \\ \vdots \\ \langle \hat{a}_L^N \hat{a}_R^{\dagger N} \hat{a}_R^N \rangle \\ \vdots \\ \langle \hat{a}_L^{\dagger N} \hat{a}_L^N \hat{a}_R^{\dagger N} \hat{a}_R^N \rangle \end{bmatrix} \tag{11}$$

We can then relate $\vec{a}$ to $\vec{S}$ by a matrix H, such that $\vec{S} = H\vec{a}$. This matrix will have dimensions $(N+1)^4 \times (N+1)^4$ and be of the form

$$H = \begin{bmatrix} 1 & 0 & 0 & \cdots & 0 & 0 & 0 \cdots 0 \\ \langle \hat{h}_R^{\dagger} \rangle & 1 & 0 & \cdots & 0 & 0 & 0 \cdots 0 \\ \langle \hat{h}_R^{\dagger 2} \rangle & 2\langle \hat{h}_R^{\dagger} \rangle & 1 & \cdots & 0 & 0 & 0 \cdots 0 \\ \vdots & \vdots & \vdots & \ddots & \vdots & \vdots & \vdots \ddots \vdots \\ \langle \hat{h}_R^{\dagger N} \rangle & \binom{N}{1}\langle \hat{h}_R^{\dagger N-1} \rangle & \binom{N}{2}\langle \hat{h}_R^{\dagger N-2} \rangle & \cdots & 1 & 0 & 0 \cdots 0 \\ \langle \hat{h}_R \rangle & 0 & 0 & \cdots & 0 & 1 & 0 \cdots 0 \\ \langle \hat{h}_R \hat{h}_R^{\dagger} \rangle & \langle \hat{h}_R \rangle & 0 & \cdots & 0 & \langle \hat{h}_R^{\dagger} \rangle & 1 \cdots 0 \\ \vdots & \vdots & \vdots & \ddots & \vdots & \vdots & \vdots \ddots \vdots \\ \langle \hat{h}_L^N \hat{h}_L^{\dagger N} \hat{h}_R^N \hat{h}_R^{\dagger N} \rangle & \binom{N}{1}\langle \hat{h}_L^N \hat{h}_L^{\dagger N} \hat{h}_R^N \hat{h}_R^{\dagger N-1} \rangle & \cdots & \cdots & \langle \hat{h}_L^N \hat{h}_L^{\dagger N} \hat{h}_R^N \rangle & \binom{N}{1}\langle \hat{h}_L^N \hat{h}_L^{\dagger N} \hat{h}_R^{N-1} \hat{h}_R^{\dagger N} \rangle & \cdots \cdots 1 \end{bmatrix} \tag{12}$$

The moments in the $\vec{a}$ can then be solved for by inverting H:$\vec{a} = H^{-1}\vec{S}$. Note that the matrix H is lower triangular, and thus, the system can be solved efficiently using back substitution.

SUPPLEMENTARY MATERIALS

Supplementary material for this article is available at http://advances.sciencemag.org/cgi/content/full/6/41/eabb8780/DC1

REFERENCES AND NOTES

1. J. I. Cirac, A. K. Ekert, S. F. Huelga, C. Macchiavello, Distributed quantum computation over noisy channels. *Phys. Rev. A* **59**, 4249 (1999).
2. H. J. Kimble, The quantum internet. *Nature* **453**, 1023–1030 (2008).
3. C. Monroe, R. Raussendorf, A. Ruthven, K. R. Brown, P. Maunz, L.-M. Duan, J. Kim, Large-scale modular quantum-computer architecture with atomic memory and photonic interconnects. *Phys. Rev. A* **89**, 022317 (2014).

4. L. Jiang, J. M. Taylor, A. S. Sørensen, M. D. Lukin, Distributed quantum computation based on small quantum registers. *Phys. Rev. A* **76**, 062323 (2007).
5. I. Afek, O. Ambar, Y. Silberberg, High-NOON states by mixing quantum and classical light. *Science* **328**, 879–881 (2010).
6. P. Kok, H. Lee, J. P. Dowling, Creation of large-photon-number path entanglement conditioned on photodetection. *Phys. Rev. A* **65**, 052104 (2002).
7. P. Walther, J.-W. Pan, M. Aspelmeyer, R. Ursin, S. Gasparoni, A. Zeilinger, De Broglie wavelength of a non-local four-photon state. *Nature* **429**, 158–161 (2004).
8. S. Saito, X. Zhu, R. Amsüss, Y. Matsuzaki, K. Kakuyanagi, T. Shimo-Oka, N. Mizuochi, K. Nemoto, W. J. Munro, K. Semba, Towards realizing a quantum memory for a superconducting qubit: Storage and retrieval of quantum states. *Phys. Rev. Lett.* **111**, 107008 (2013).
9. P. Kurpiers, P. Magnard, T. Walter, B. Royer, M. Pechal, J. Heinsoo, Y. Salathé, A. Akin, S. Storz, J.-C. Besse, S. Gasparinetti, A. Blais, A. Wallraff, Deterministic quantum state transfer and remote entanglement using microwave photons. *Nature* **558**, 264–267 (2018).
10. N. Leung, Y. Lu, S. Chakram, R. K. Naik, N. Earnest, R. Ma, K. Jacobs, A. N. Cleland, D. I. Schuster, Deterministic bidirectional communication and remote entanglement generation between superconducting qubits. *npj Quantum Inf.* **5**, 18 (2019).
11. R. Barends, J. Kelly, A. Megrant, A. Veitia, D. Sank, E. Jeffrey, T. C. White, J. Mutus, A. G. Fowler, B. Campbell, Y. Chen, Z. Chen, B. Chiaro, A. Dunsworth, C. Neill, P. O'Malley, P. Roushan, A. Vainsencher, J. Wenner, A. N. Korotkov, A. N. Cleland, J. M. Martinis, Superconducting quantum circuits at the surface code threshold for fault tolerance. *Nature* **508**, 500–503 (2014).
12. F. Arute, K. Arya, R. Babbush, D. Bacon, J. C. Bardin, R. Barends, R. Biswas, S. Boixo, F. G. S. L. Brandao, D. A. Buell, B. Burkett, Y. Chen, Z. Chen, B. Chiaro, R. Collins, W. Courtney, A. Dunsworth, E. Farhi, B. Foxen, A. Fowler, C. Gidney, M. Giustina, R. Graff, K. Guerin, S. Habegger, M. P. Harrigan, M. J. Hartmann, A. Ho, M. Hoffmann, T. Huang, T. S. Humble, S. V. Isakov, E. Jeffrey, Z. Jiang, D. Kafri, K. Kechedzhi, J. Kelly, P. V. Klimov, S. Knysh, A. Korotkov, F. Kostritsa, D. Landhuis, M. Lindmark, E. Lucero, D. Lyakh, S. Mandrà, J. R. McClean, M. McEwen, A. Megrant, X. Mi, K. Michielsen, M. Mohseni, J. Mutus, O. Naaman, M. Neeley, C. Neill, M. Y. Niu, E. Ostby, A. Petukhov, J. C. Platt, C. Quintana, E. G. Rieffel, P. Roushan, N. C. Rubin, D. Sank, K. J. Satzinger, V. Smelyanskiy, K. J. Sung, M. D. Trevithick, A. Vainsencher, B. Villalonga, T. White, Z. J. Yao, P. Yeh, A. Zalcman, H. Neven, J. M. Martinis, Quantum supremacy using a programmable superconducting processor. *Nature* **574**, 505–510 (2019).
13. A. A. Abdumalikov Jr., O. V. Astafiev, Y. A. Pashkin, Y. Nakamura, J. S. Tsai, Dynamics of coherent and incoherent emission from an artificial atom in a 1D space. *Phys. Rev. Lett.* **107**, 043604 (2011).
14. I.-C. Hoi, T. Palomaki, G. Johansson, J. Lindkvist, P. Delsing, C. M. Wilson, Generation of nonclassical microwave states using an artificial atom in 1D open space. *Phys. Rev. Lett.* **108**, 263601 (2012).
15. P. Forn-Díaz, C. W. Warren, C. W. S. Chang, A. M. Vadiraj, C. M. Wilson, On-demand microwave generator of shaped single photons. *Phys. Rev. Applied* **8**, 054015 (2017).
16. A. González-Tudela, V. Paulisch, D. E. Chang, H. J. Kimble, J. I. Cirac, Deterministic generation of arbitrary photonic states assisted by dissipation. *Phys. Rev. Lett.* **115**, 163603 (2015).
17. W. Pfaff, C. J. Axline, L. D. Burkhart, U. Vool, P. Reinhold, L. Frunzio, L. Jiang, M. H. Devoret, R. J. Schoelkopf, Controlled release of multiphoton quantum states from a microwave cavity memory. *Nat. Phys.* **13**, 882–887 (2017).
18. S. Gasparinetti, M. Pechal, J.-C. Besse, M. Mondal, C. Eichler, A. Wallraff, Correlations and entanglement of microwave photons emitted in a cascade decay. *Phys. Rev. Lett.* **119**, 140504 (2017).
19. J. Koch, T. M. Yu, J. Gambetta, A. A. Houck, D. I. Schuster, J. Majer, A. Blais, M. H. Devoret, S. M. Girvin, R. J. Schoelkopf, Charge-insensitive qubit design derived from the Cooper pair box. *Phys. Rev. A* **76**, 042319 (2007).
20. A. F. van Loo, A. Fedorov, K. Lalumière, B. C. Sanders, A. Blais, A. Wallraff, Photon-mediated interactions between distant artificial atoms. *Science* **342**, 1494–1496 (2013).
21. K. Lalumière, B. C. Sanders, A. F. van Loo, A. Fedorov, A. Wallraff, A. Blais, Input-output theory for waveguide QED with an ensemble of inhomogeneous atoms. *Phys. Rev. A* **88**, 043806 (2013).
22. C. Eichler, D. Bozyigit, C. Lang, L. Steffen, J. Fink, A. Wallraff, Experimental state tomography of itinerant single microwave photons. *Phys. Rev. Lett.* **106**, 220503 (2011).
23. C. M. Caves, Quantum limits on noise in linear amplifiers. *Phys. Rev. D* **26**, 1817 (1982).
24. C. Eichler, D. Bozyigit, A. Wallraff, Characterizing quantum microwave radiation and its entanglement with superconducting qubits using linear detectors. *Phys. Rev. A* **86**, 032106 (2012).
25. C. K. Hong, Z. Y. Ou, L. Mandel, Measurement of subpicosecond time intervals between two photons by interference. *Phys. Rev. Lett.* **59**, 2044 (1987).
26. C. Lang, C. Eichler, L. Steffen, J. M. Fink, M. J. Woolley, A. Blais, A. Wallraff, Correlations, indistinguishability and entanglement in Hong-Ou-Mandel experiments at microwave frequencies. *Nat. Phys.* **9**, 345–348 (2013).
27. A. Frisk Kockum, P. Delsing, G. Johansson, Designing frequency-dependent relaxation rates and Lamb shifts for a giant artificial atom. *Phys. Rev. A* **90**, 013837 (2014).
28. B. Kannan, M. J. Ruckriegel, D. L. Campbell, A. F. Kockum, J. Braumüller, D. Kim, M. Kjaergaard, P. Krantz, A. Melville, B. M. Niedzielski, A. Vepsalainen, R. Winik, J. Yoder, F. Nori, S. Gustavsson, W. D. Oliver, Waveguide quantum electrodynamics with superconducting artificial giant atoms. *Nature* **583**, 775–779 (2020).
29. J. P. Dowling, Quantum optical metrology – The low-down on high-N00N states. *Contemp. Phys.* **49**, 125 (2008).
30. B. Royer, A. L. Grimsmo, A. Choquette-Poitevin, A. Blais, Itinerant microwave photon detector. *Phys. Rev. Lett.* **120**, 203602 (2018).
31. S. Kono, K. Koshino, Y. Tabuchi, A. Noguchi, Y. Nakamura, Quantum non-demolition detection of an itinerant microwave photon. *Nat. Phys.* **14**, 546–549 (2018).
32. N. Gheeraert, S. Kono, Y. Nakamura, Bidirectional emitter and receiver of itinerant microwave photons in a waveguide. arXiv:2004.01924 (2020).
33. C. Macklin, K. O'Brien, D. Hover, M. E. Schwartz, V. Bolkhovsky, X. Zhang, W. D. Oliver, I. Siddiqi, A near–quantum-limited Josephson traveling-wave parametric amplifier. *Science* **350**, 307–310 (2015).
34. I.-C. Hoi, C. M. Wilson, G. Johansson, T. Palomaki, B. Peropadre, P. Delsing, Demonstration of a single-photon router in the microwave regime. *Phys. Rev. Lett.* **107**, 073601 (2011).
35. O. Astafiev, A. M. Zagoskin, A. A. Abdumalikov Jr., Y. A. Pashkin, T. Yamamoto, K. Inomata, Y. Nakamura, J. S. Tsai, Resonance fluorescence of a single artificial atom. *Science* **327**, 840–843 (2010).
36. I.-C. Hoi, C. M. Wilson, G. Johansson, J. Lindkvist, B. Peropadre, T. Palomaki, P. Delsing, Microwave quantum optics with an artificial atom in one-dimensional open space. *New J. Phys.* **15**, 025011 (2013).
37. M. Mirhosseini, E. Kim, X. Zhang, A. Sipahigil, P. B. Dieterle, A. J. Keller, A. Asenjo-Garcia, D. E. Chang, O. Painter, Cavity quantum electrodynamics with atom-like mirrors. *Nature* **569**, 692–697 (2019).

Acknowledgments: We thank J. Braumüller and A. Vepsäläinen for the valuable discussions. **Funding:** This research was funded in part by the U.S. Department of Energy, Office of Science, Basic Energy Sciences, Materials Sciences and Engineering Division under contract no. DE-AC02-05-CH11231 within the High-Coherence Multilayer Superconducting Structures for Large Scale Qubit Integration and Photonic Transduction program (QISLBNL), and by the Department of Defense via MIT Lincoln Laboratory under U.S. Air Force contract no. FA8721-05-C-0002. B.K. gratefully acknowledges support from the National Defense Science and Engineering Graduate Fellowship program. M.K. gratefully acknowledges support from the Carlsberg Foundation during a portion of this work. **Author contributions:** B.K., D.L.C., S.G., and W.D.O. conceived and designed the experiment. D.L.C. designed the devices. B.K. and D.L.C. conducted the measurements, and B.K., D.L.C., and F.V. analyzed the data. D.K.K., A.M., B.M.N., and J.L.Y. performed sample fabrication. B.K. and D.L.C. wrote the manuscript. M.K., P.K., and R.W. assisted with the experimental setup. T.P.O., S.G., and W.D.O. supervised the project. All authors discussed the results and commented on the manuscript. **Competing interests:** The authors declare that they have no competing interests. **Data and materials availability:** The data and code that support the findings of this study are available from the corresponding author upon reasonable request. All data needed to evaluate the conclusions in the paper are present in the paper and/or the Supplementary Materials. Additional data related to this paper may be requested from the authors.

Submitted 24 March 2020
Accepted 21 August 2020
Published 7 October 2020
10.1126/sciadv.abb8780

Citation: B. Kannan, D. L. Campbell, F. Vasconcelos, R. Winik, D. K. Kim, M. Kjaergaard, P. Krantz, A. Melville, B. M. Niedzielski, J. L. Yoder, T. P. Orlando, S. Gustavsson, W. D. Oliver, Generating spatially entangled itinerant photons with waveguide quantum electrodynamics. *Sci. Adv.* **6**, eabb8780 (2020).

Science Advances

Generating spatially entangled itinerant photons with waveguide quantum electrodynamics

B. Kannan, D. L. Campbell, F. Vasconcelos, R. Winik, D. K. Kim, M. Kjaergaard, P. Krantz, A. Melville, B. M. Niedzielski, J. L. Yoder, T. P. Orlando, S. Gustavsson and W. D. Oliver

Sci Adv **6** (41), eabb8780.
DOI: 10.1126/sciadv.abb8780